A COMPREHENSIVE STUDY OF THE MICROWAVE INSTABILITY*

A. Blednykh[†], B. Bacha, G. Bassi, O. Chubar, M. Rakitin, V. Smaluk, M. Zhernenkov
BNL, NSLS-II, Upton, NY, 11973-5000, USA

Abstract

Several instability thresholds and special waveform beam patterns have been observed during measurements of the horizontal beam size change vs. single bunch current by the synchrotron light monitor (SLM) camera installed in a low dispersion area of the NSLS-II storage ring. The electron beam energy spread from the In-Vacuum Undulator (IVU) of the Soft Matter Interfaces (SMI) beam line confirmed the microwave beam pattern behaviour as a current dependent effect. The numerically obtained total longitudinal wakepotential by the GdfidL code allowed us to compare the measured results with particle tracking simulations using the SPACE code. The instability thresholds behaviour at different RF voltages are in some sort of overarching agreement.

SLM AND IVU SPECTRA MEASUREMENTS

The new generations of storage ring light sources do not offer any reduction of another important "part" of the full 6-dimensional electron beam emittance – the energy spread. Electron beam energy spread is an important limiting factor for the peak flux at spectral harmonics of undulators – the main insertion devices used as radiation sources in these storage rings. Besides reducing the spectral flux, especially at high undulator radiation harmonics that are extensively used for producing X-rays in medium-energy storage rings, the electron beam energy spread affects angular divergence of the emitted radiation, and can represent a significant obstacle for the increase of undulator radiation brightness in future ultra-low-emittance storage ring based sources. A detailed study of electron beam energy spread in different operation regimes represents a very important topic of electron beam dynamics studies in storage ring facilities.

Two diagnostic methods have been applied to measure the longitudinal microwave beam instability thresholds and its microwave pattern behaviour in the NSLS-II storage ring: 1) the horizontal beam-profile change versus single bunch current has been monitored by a SLM camera installed in a low dispersion area [1], and 2) the In-Vacuum Undulator (IVU) of the Soft Matter Interfaces (SMI) beam line [2] has been used as a diagnostic tool to determine the full width at half maximum (FWHM) change as a function of current based on the IVU spectrum of 7th harmonic.

Horizontal beam size and FHWM of IVU spectra as a function of single bunch current are shown in Fig. 1 for two different lattices: 1) bare lattice (BL), with all insertion devices (IDs) magnet gap open and 2) 3DW lattice,

with all IDs magnet gap closed. Measurements by the SLM camera were done during different studies time and they are repeatable. The designed energy spread (in the limit of zero beam intensity) in NSLS-II can be varied by closing and opening the magnet gaps of three 7m damping wigglers (DWs) installed in Cell 08, 18, 28 [3].
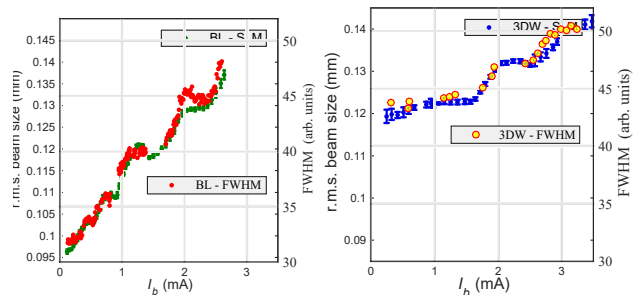

Figure 1: Horizontal beam size change measurements from SLM camera and FWHM measured form the IVU spectrum of 7th harmonic at $V_{RF} = 2.6MV$ for the two different lattices BL and 3DW.

IMPEDANCE BUDGET ($\bar{\sigma}_s = 0.3mm$)

To predict the longitudinal instability thresholds and bunch lengthening induced by the potential well distortion, the longitudinal wakepotential $W_{||}(s)$ is numerically calculated as a sum of the contributions due to vacuum chamber components distributed around the ring (Fig. 2a). An approximation to the wakepotential for a $\bar{\sigma}_s = 0.3mm$ charge distribution length, much shorter than the length of the unperturbed circulating bunch is used as a pseudo-Green's function for beam dynamic simulations (Fig. 2b).
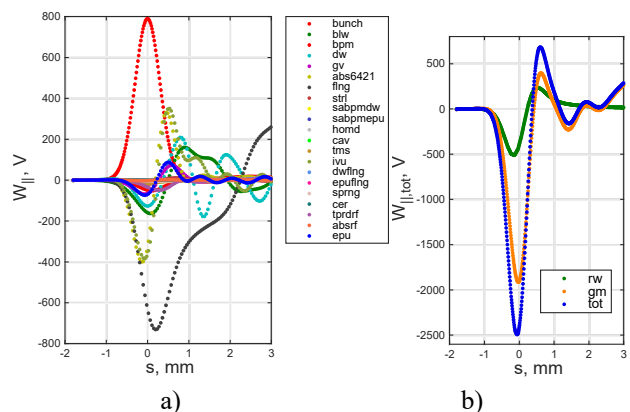

Figure 2: The longitudinal short-range wakepotential calculated for a $\bar{\sigma}_s = 0.3mm$ bunch length. a) $W_{||}(s)$ calculated for each individual vacuum component and multiplied by a total number. b) The total longitudinal wakepotential $W_{||,tot}(s)$ of the NSLS-II storage ring as a sum of geometric and resistive wall wakepotentials.

The 3D GdfidL numerical code has been used for the wakepotential simulations [4]. Not all vacuum compo-

nents are included yet into the impedance budget. Geometric impedance of 7 flange absorbers with different profiles and resistive wall of 8 long straight-section and 7 short straight-section are under analysis. To keep track of changes the total longitudinal wakepotential file has been released (WMay82017.txt) and will be updated with more components added. As can be seen from Fig. 2a, the main contribution to the total longitudinal wakepotential is due to ~750 RF shielded flange joints (black doted trace). A secondary contributor is the flange absorber (dark yellow trace) with a ~115 total number and 9 IVUs presently installed.

COMPARISON WITH SIMULATIONS

In this Section we compare SLM measurements with particle tracking simulations using the SPACE code [5]. To this end, the computed total longitudinal wakepotential $W_{\|,tot}$ (Fig. 2b) was uploaded as input file in SPACE.
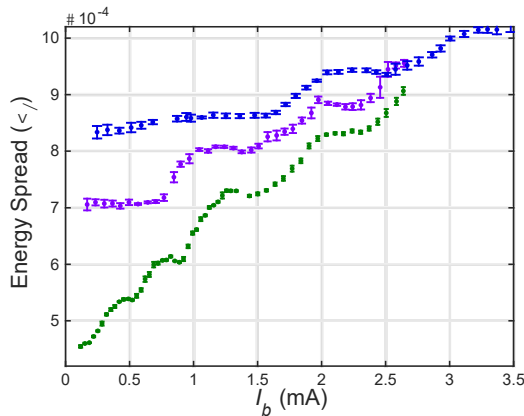

Figure 3: Energy spread vs single bunch current calculated from SLM camera bunch size measurements for the three different lattices BL, 1DW and 3DW at $V_{RF} = 2.6MV$.

Since SLM measurements give the horizontal bunch size and SPACE simulations the energy spread, to compare the results we use both $\sigma_x = \sqrt{\varepsilon_x \beta_x + (\eta_x \sigma_\delta)^2}$ [6] and its inverse $\sigma_\delta = \sqrt{\sigma_x^2 - \varepsilon_x \beta_x}/\eta_x$, where ε_x is the horizontal emittance with design values $\varepsilon_x = 0.9nm$ (3DW), $\varepsilon_x = 1.4nm$ (1DW) and $\varepsilon_x = 2.2nm$ (BL), β_x is the horizontal beta function and η_x the horizontal dispersion with design values $\beta_x = 2.77m$ and $\eta_x = 0.13m$.

The several instability thresholds observed in the measurements (Fig. 3) are seen in the particle tracking simulations as well (Fig. 4 and Fig. 6 for the 3DW lattice and $V_{RF} = 3.4MV$). Fig. 4a shows numerical simulations of the energy spread vs. number of turns for several single bunch currents above the microwave instability threshold 1.65mA. Different instability regimes are seen, characterized by the transition currents $I_b = 1.65mA$ (microwave instability threshold), $I_b = 2.35mA$ and $I_b = 2.5mA$, as shown in Fig. 4b, where the numerical simulations are

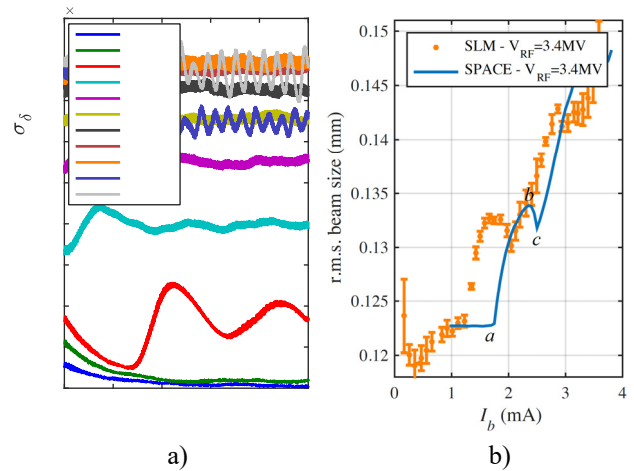a)   b)

Figure 4: SPACE simulations for 3DW lattice and comparison with SLM measured data at $V_{RF} = 3.4MV$. a) Turn-by-turn energy spread for different values of single-bunch current. b) Horizontal beam size change as a function of single-bunch current. Orange dots with error bars are SLM data and the blue trace is the maximum amplitude (over the last 5000 turns) of the energy oscillations from Fig. 4a.
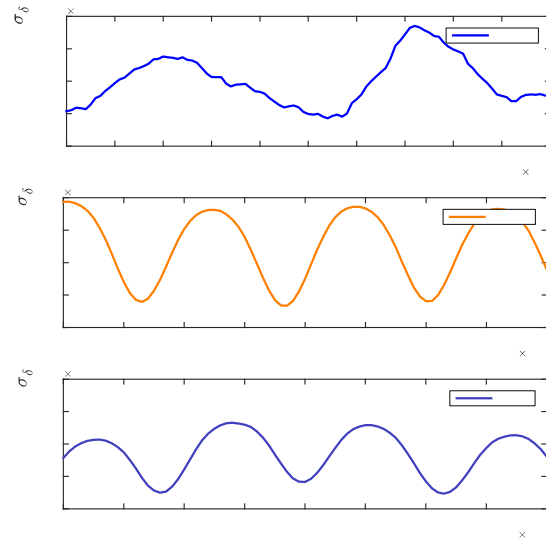

Figure 5: Zoomed part of the energy oscillations from Fig. 4a for three highlighted regimes shown on Fig. 4b: a) $I_b = 1.65mA$ blue trace, b) $I_b = 2.35mA$ orange trace and c) $I_b = 2.5mA$ dark blue trace.

represented by the blue trace and the horizontal beam size measurements from SLM by the orange dots with error bars. The time evolution of the energy spread over the last 100 turns is shown in Fig. 5 for the three transition currents. It is clearly seen the presence of a higher order mode of oscillation with frequency $4f_s$ (~25 turns), where f_s is the synchrotron frequency, above the microwave instability threshold, absent at $I_b = 1.65mA$ (a), where only the natural mode of oscillation of the energy spread, $2f_s$, is present. At the current $I_b = 2.35mA$ (b), the mode of oscillation $4f_s$ has the maximum, then starts to decrease approaching the current $I_b = 2.5mA$ (c), thus ex-

plaining the apparent reduction in the energy spread. Fig. 6 shows the same comparison of Fig. 4b at $V_{RF} = 2.6MV$.
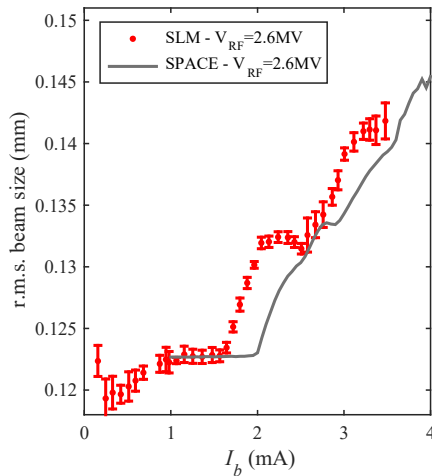

Figure 6: Horizontal beam size change as a function of single-bunch current for the 3DW lattice at RF voltage $V_{RF} = 2.6MV$.

Streak camera bunch lengthening measurements as a function of single bunch current for the bare lattice (BL) and for 3DW lattice [7,8] are presented in Fig. 7 at $V_{RF} = 3.4MV$. The simulated bunch lengthening for the 3DW lattice is smaller than the measured one, by a factor of 1.3 at high current. Further simulations show that the rate of increase of the bunch length approaches the measured values with more vacuum components added.

In Fig. 8, we summarize the measured instability thresholds vs. sb current at different RF voltages [9]. The first microwave instability threshold depends on the RF voltage as $I_{th1} \sim 1/\sqrt{V_{RF}}$, which is consistent with the Boussard criterion [10]. The red dots represent the measurements and the blue curve the I_{th}^2 fit to the data.
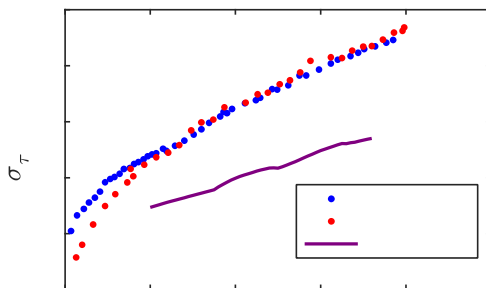

Figure 7: Bunch lengthening dependence on single-bunch current I_b. Comparison of numerical simulations vs measured results made by the streak camera at $V_{RF} = 3.4MV$ for bare lattice and for regular operational lattice with 3DWs magnet gap closed.

The main difficulty during the set of measurements was to obtain less noisy microwave beam size pattern change in order to determine accurately the first instability threshold current I_{th1} at some RF voltages. Separation between two thresholds, I_{th1} and I_{th2}, can be very tiny. The first instability threshold can be smoothed out if the measurements are noisy or two thresholds are close to each other and I_{th2} can be picked up as the first one. Higher-order instability thresholds are combined to different groups with a linear pattern. The slope of a pattern group is increased with V_{RF}.
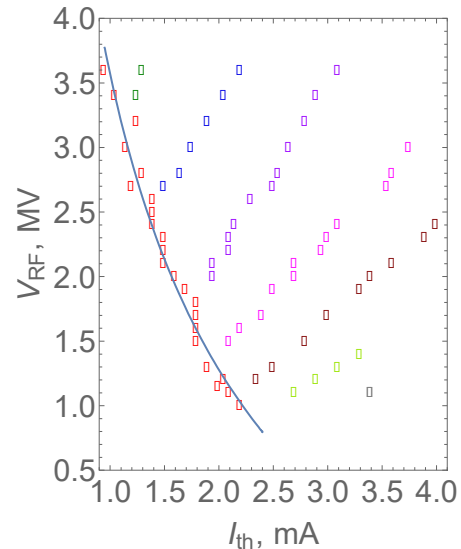

Figure 8: Summary of the measured single-bunch instability thresholds at different RF voltages. Red dots represent the first microwave instability threshold behavior. Blue curve is a fit to $1/\sqrt{V_{RF}}$.

ACKNOWLEDGMENT

REFERENCES

[1] W. Cheng, in *Proceedings of BIW10*, Santa Fe, New Mexico, USA, paper TUPSM110.

[2] M. Zhernenkov *et al.*, *Proc. Spie*, vol. 9209, p. 92090G, 2014

[3] Brookhaven National Laboratory, 2006, NSLS-II Conceptual Design Report.

[4] W. Bruns, http://www.gdfidl.de

[5] G. Bassi, A. Blednykh and V. Smaluk, *Phys. Rev. Acc. and Beams* 19, 024401 (2016)

[6] H. Wiedemann, Particle Accelerator Physics Book, Springer, Berlin Heidelberg, New York, 2007

[7] A. Blednykh, et al., in *Proceedings of IPAC2015*, Richmond, VA, USA, paper TUAB2.

[8] W. Cheng *et al.*, in *Proceedings of IBIC2015*, Melbourne, Australia, 2015, paper MOPB083.

[9] A. Blednykh *et al.*, in *Proceedings of NAPAC2016*, Chicago, IL, USA, paper WEA1C005

[10] D. Boussard, CERN LABII/RF/INT/75-2 (1975).